TOP PHYSICS AT CDF

Richard E. Hughes*
Department of Physics and Astronomy
University of Rochester
Rochester, New York 14627

Representing the CDF Collaboration

ABSTRACT

We report on top physics results using a 100 pb^{-1} data sample of $p\bar{p}$ collisions at $\sqrt{s} = 1.8\ TeV$ collected with the Collider Detector at Fermilab (CDF). We have identified top signals in a variety of decay channels, and used these channels to extract a measurement of the top mass and production cross section. A subset of the data (67 pb^{-1}) is used to determine $M_{top} = 176 \pm 8(stat) \pm 10(syst)$ and $\sigma(t\bar{t}) = 7.6\ ^{+2.4}_{-2.0}\ pb$. We present studies of the kinematics of $t\bar{t}$ events and extract the first direct measurement of V_{tb}. Finally, we indicate prospects for future study of top physics at the Tevatron.

*Supported by Department of Energy Grant No. DE-FG02-91ER40685.

1 Introduction

1.1 Indirect Information on Top

Much of our indirect information on the existence of the top quark has come from studying the bottom quark. By studying the forward-backward asymmetry A_{FB} $(e^+e^- \rightarrow b\bar{b})$ at low energy,[1] and at the Z^0 resonance, combined with the partial width Γ $(Z^0 \rightarrow b\bar{b})$ (Ref. 2), one can determine that the weak-isospin of the b quark is consistent with $T_3 = -\frac{1}{2}$. In addition, the absence of decays such as $b \rightarrow sl^+l^-$ (at a rate comparable to $b \rightarrow cl^-\nu$) can be explained if the b quark is a member of an SU(2) doublet.[3] Finally, cancellation of anomalies requires that the electric charges in each generation sum to zero. By definition, the top quark is the $T_3 = +\frac{1}{2}$ weak isospin partner to the b quark.

Given fits to electroweak observables from LEP and SLC, that also include information from neutrino scattering, and the measurement of M_W from $p\bar{p}$ colliders, one obtains[2] a favored value for the top mass of $M_{top} = 178\ ^{+11}_{-11}\ ^{+18}_{-19}\ GeV/c^2$. This value is obtained assuming a value for the Higgs mass of $M_H = 300\ GeV/c^2$. The first uncertainty is experimental, while the second comes from varying the Higgs mass over the range of 60 to 1000 GeV/c^2. If instead one leaves the Higgs mass free in the fit, the resulting top mass is $M_{top} = 156\ ^{+14}_{-15}\ GeV/c^2$ (Ref. 4).

1.2 Direct Searches for Top

A number of direct searches for the top quark have been performed at $p\bar{p}$ colliders. In 1990, CDF obtained a limit[5] of $M_{top} > 91\ GeV/c^2$ at 95 % CL. In 1993, DØ obtained a limit[6] of $M_{top} > 131\ GeV/c^2$ at 95 % CL. The first evidence for top-quark production was obtained by CDF in 1994 (Ref. 7). In that analysis, we found a 2.8σ excess of signal over the expectation from background, using a data sample with an integrated luminosity of $19.3 \pm 0.7\ pb^{-1}$ (referred to as the Run 1A sample). The interpretation of the excess as top-quark production was supported by a peak in the mass distribution for fully reconstructed events. Additional evidence was found in the jet energy distributions in lepton + jet events.[8]

A second collider run took place from January 1994 until June 1995. This is referred to as Run 1B and yielded an additional $\sim 90\ pb^{-1}$ of data. On March 2nd, 1995, both the CDF[9] and DØ (Ref. 10) Collaborations reported observation of the top quark, using the Run 1A data plus a subset of the Run 1B data set. In the remainder of this document, we will describe the CDF results, including an updated Run 1B data set.

1.3 Top Production and Decay

In $p\bar{p}$ collisions, top quarks are pair produced by gluon-gluon fusion and $q\bar{q}$ annihilation. The relative importance of the two processes is dependent on the mass of the top quark. For $M_{top} = 175\ GeV/c^2$, one expects approximately 90% of the rate from $q\bar{q}$ annihilation. The $t\bar{t}$ production cross section has been calculated at next-to-leading order, with the inclusion of diagrams due to soft gluon emission.[11] The result is shown in Fig. 1. The dashed curves in this figure represent the uncertainties obtained in varying parameters related to the perturbative part of the cross-section calculation. They do not represent the full uncertainty in the central value of the cross section, which could be as large as 30% (Ref. 12).

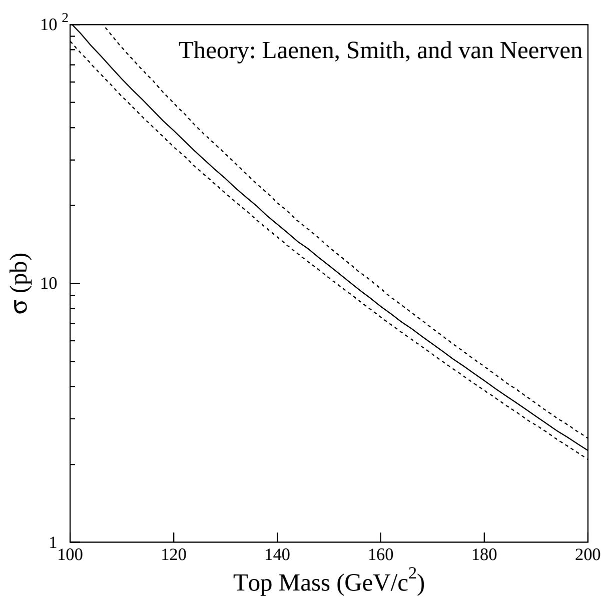

Fig. 1. The theory cross section for $t\bar{t}$ production.

For top masses greater than the combined mass of the W boson and the b quark, the top quark is expected to decay almost exclusively to a real W and a b. The $t\bar{t}$ decay signature is then determined by how the two W bosons in the event decay, as shown in Fig. 2. There are three primary signatures:

- Both W's Decay $W \to \ell\nu$

  In this case, the final state is $\ell^+ \ \nu\ell^- \ \nu b\bar{b}$, where ℓ is an electron or a muon. This is referred to as the dilepton channel. The branching ratio is approximately 5%.

- One W Decays $W \to \ell\nu$

  In this case, the final state is $\ell^+\nu \ q\bar{q}' \ \ b\bar{b}$. This is referred to as the lepton plus jets channel, and the branching ratio is $\sim 30\%$.

- Both W's decay $W \to q\bar{q}'$

  In this case, the final state is $q\bar{q}' \ q\bar{q}' \ \ b\bar{b}$. This is referred to as the all-hadronic channel, and the branching ratio is $\sim 44\%$.

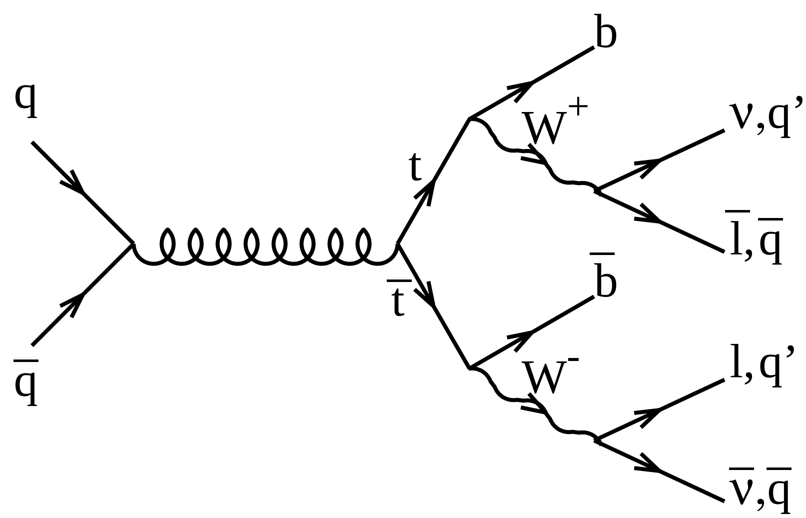

Fig. 2. Tree level $t\bar{t}$ production via $q\bar{q}$ annihilation, followed by the Standard Model decay chain.

1.4 The CDF Detector

The CDF detector is a general-purpose detector designed to study the physics of $p\bar{p}$ collisions. It has both azimuthal and forward-backward symmetry. A side-view cross section of the CDF detector is shown in Fig. 3. The CDF detector consists of a magnetic spectrometer surrounded by calorimeters and muon chambers.[13] A new low-noise, radiation-hard, four-layer silicon vertex detector (SVX), located immediately outside the beampipe, provides precise track reconstruction in the plane transverse to the beam and is used to identify secondary vertices from b and c quark decays.[14] The momenta of charged particles are measured in the central tracking chamber (CTC), which is in a 1.4 T superconducting solenoidal magnet. Outside the CTC, electromagnetic and hadronic calorimeters cover the pseudorapidity region $|\eta| < 4.2$ (Ref. 15), and are used to identify jets and electron candidates. The calorimeters are also used to measure the missing transverse energy, $\not\!\!E_T$, which can indicate the presence of undetected energetic neutrinos. Outside the calorimeters, drift chambers in the region $|\eta| < 1.0$ provide muon identification. A three-level trigger selects the inclusive electron and muon events used in this analysis.

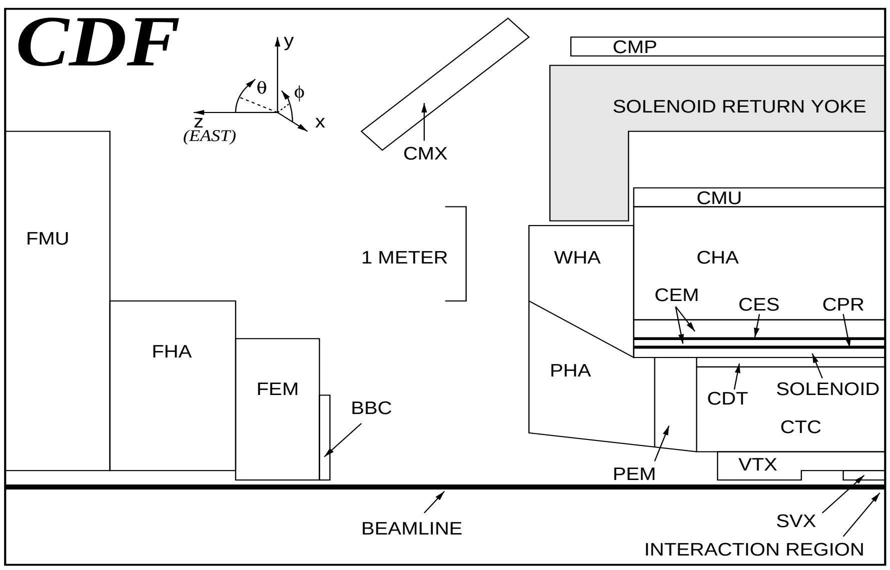

Fig. 3. A side view of the CDF detector. The detector is forward-backward symmetric about the interaction region, which is at the lower-right corner of the figure.

2 The Dilepton Channel

The dilepton selection is based on the expected decay topology $t\bar{t} \rightarrow W^+bW^-\bar{b} \rightarrow \ell^+\nu\ell^-\nu b\bar{b}$, where ℓ is an electron or muon. We require that each event contains at least one primary, isolated electron (muon) with E_T (P_T) ≥ 20 GeV (GeV/c). Electrons consistent with photon conversions are removed. In addition, $Z \rightarrow e^+e^-$ ($\mu^+\mu^-$) are removed if the invariant mass of the lepton pair is in the range of 75 to 105 GeV/c^2. For the secondary lepton, the same E_T (P_T) cut is applied, but a slightly looser set of identification cuts are imposed. It must have a charge opposite in sign to that of the primary lepton.

Since there are two remaining b quarks in the final state, we require that each event contain at least two jets, with uncorrected $E_T \geq 10$ GeV and $|\eta| < 2.0$. The presence of two ν's from the decay of the W bosons motivates a cut on the missing energy $\not{E}_T \geq 25$ GeV. An additional cut is applied for the backgrounds of $Z \rightarrow \tau^+\tau^-$ and Drell-Yan. In these events, $\not{E}_T$ can be generated along the direction of the leptons (from the τ decay ν's) or along the direction of the jets (from mismeasurement of jet energies). To reduce this background, we require $\not{E}_T \geq 50$ GeV, when the azimuthal angle between the $\not{E}_T$ and the nearest jet or lepton is $< 20°$.

After all cuts, the relative acceptance among the three possible dilepton categories is 57% for $e\mu$, 28% for $\mu\mu$, and 15% for ee (for a top mass of 175 GeV/c^2). The expected number of events (using the central value of the theoretical cross section) from $t\bar{t}$ passing all cuts is shown in Table 1, for a luminosity of 100 pb^{-1}.

Top Mass (GeV/c^2)	$\sigma_{t\bar{t}}$ (pb)	Expected Events (#)
160	8.2	6.6
170	5.8	4.5
180	4.2	3.6

Table 1. The predicted central value of the $t\bar{t}$ production cross section from Laenen *et al.*, and the number of dilepton $t\bar{t}$ events expected after all cuts, as a function of top-quark mass.

The backgrounds to the dilepton channel are, in order of importance, Drell-Yan, $p\bar{p} \to Z \to \tau\tau$, fake leptons, $p\bar{p} \to WW$, and $p\bar{p} \to b\bar{b}$. The first three are calculated primarily from the data, while the last two come primarily from Monte Carlo. The individual backgrounds are given in Table 2 and yield a total background of 1.9 ± 0.3.

Category	Expected Events
Drell-Yan	0.70±0.27
$p\bar{p} \to Z \to \tau\tau$	0.56±0.11
Fake leptons	0.35±0.11
$p\bar{p} \to WW$	0.31±0.10
$p\bar{p} \to b\bar{b}$	0.03±0.02
Total	1.9±0.3

Table 2. Number of background events expected in 100 pb^{-1}, broken down by category.

We observe a total of nine events in 100 pb^{-1}. There are six $e\mu$ events, two $\mu\mu$ events, and one ee event, consistent with the relative acceptance quoted earlier. Figures 4, 5, and 6 show plots of $\Delta\phi\,(lepton\ or\ jet, \not{E}_T)$ vs. $\not{E}_T$ for the candidates. One of the $\mu\mu$ events is consistent with the radiative decay $Z \to \mu\mu\gamma$, where the γ is reconstructed as a jet (with large electromagnetic fraction). Although the background expected from this process is small ($\sim$ 0.1 event), and included in the background estimate above, we remove this event from the total sample and are left with eight events passing all selection criteria. The probability of the background estimate fluctuating to the number of observed events or more is $\mathcal{P}$ = 1 x 10^{-3}.

As described in the next section, we have two methods for identifying b jets at CDF. Although we do not require b-tagging in the dilepton channel, we note that three of the eight events have one or more b-tagged jets, providing evidence for W^+W^-b, as expected from $t\bar{t}$ production.

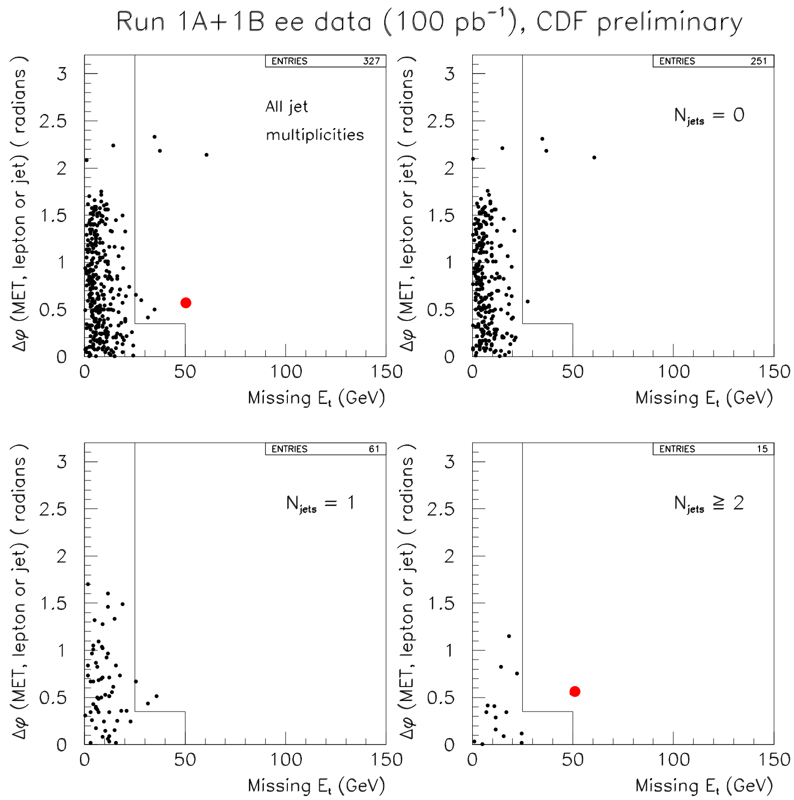

Fig. 4. The azimuthal angle between the $\not{E}_T$ and the closest lepton or jet vs. $\not{E}_T$ for the *ee* candidates. Upper left: all-jet multiplicities. Upper right: zero-jet events. Lower left: one-jet events. Lower right: $\geq$ 2-jet events (signal region).

3 The Lepton Plus Jets Channel

The lepton plus jets selection is based on the expected decay topology $t\bar{t} \rightarrow \ell\nu bq\bar{q}'\bar{b}$. Once again, we require that each event contain one isolated electron (muon) with E_T $(P_T) \geq 20$ GeV (GeV/c). The requirements on this lepton are the same as in the dilepton selection. We also require that $\not{E}_T \geq$ 20 GeV. Since there are four partons in the final state, we require that each event have $\geq$ 3 jets, with $E_T \geq 15$ GeV, and $|\eta| \leq 2.0$. The three-jet requirement is approximately 75% efficient for $M_{top} = 175$ GeV/c^2, but strongly suppresses inclusive QCD W production, as shown in Fig. 7. Any events which also pass the dilepton selection criteria are explicitly removed at this point, to keep the two search channels statistically independent.

At this stage in the selection, 296 events remain. For $M_{top} = 175$ GeV/c^2, the theoretical cross section is $\sigma_{t\bar{t}} = 4.8$ pb, and thus, we only expect ≈ 40 $t\bar{t}$ events after all cuts. Additional background rejection is still needed.

The dominant background in a lepton plus jets search is non-top QCD W + multijet production. We reject this background using b-tagging, since every $t\bar{t}$ event

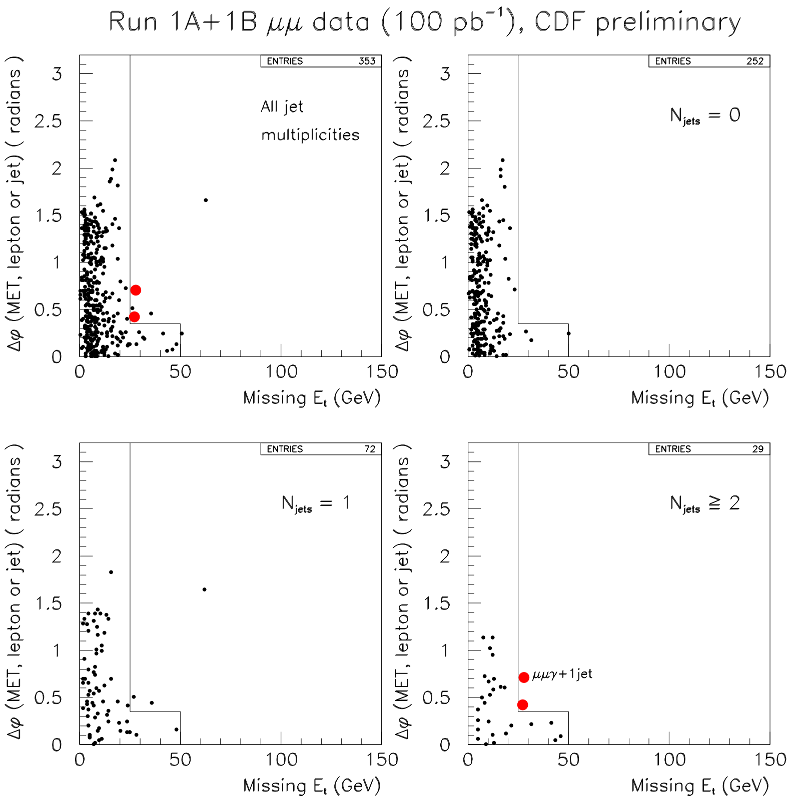

Fig. 5. The azimuthal angle between the $\not{E}_T$ and the closest lepton or jet vs. $\not{E}_T$ for the $\mu\mu$ candidates. Upper left: all-jet multiplicities. Upper right: zero-jet events. Lower left: one-jet events. Lower right: $\geq$ 2-jet events (signal region).

contains two b quarks, while only $\sim 2\%$ of QCD W + jets events are expected to contain b quarks. We identify or tag b quarks using two methods at CDF: the first requires the location of a displaced vertex using the SVX, and the second requires a soft lepton (e or μ) from b-quark decay.

3.1 Silicon Vertex Tagging

The primary method used for identifying b quarks in top events utilizes the Silicon Vertex Detector and is therefore referred to as SVX-tagging. The method relies on the excellent SVX hit resolution of $\sim 8.5\ \mu m$ per point, as shown in Fig. 8. This in turn yields an expected resolution on the impact parameter of charged tracks of $\sigma_d \sim 16(1 + (\frac{0.8}{P_T})^2)\ \mu m$, where the second term is due to multiple scattering, and P_T is the transverse momentum of the track.

The b lifetime is approximately 450 μm. This, along with the large boost the b receives in the decay of the top quark, yields a displacement in the lab frame which can be quite large. In Fig. 9, we show the transverse decay length in the lab frame of b hadrons from top decay ($M_{top} = 160\ GeV/c^2$). Note that this is before

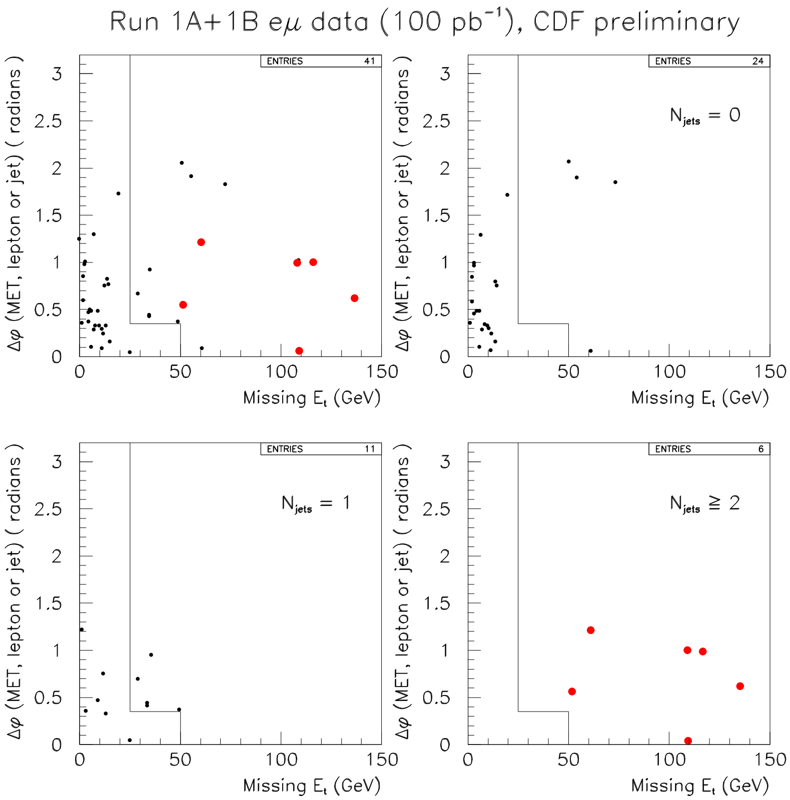

Fig. 6. The azimuthal angle between the $\not{E}_T$ and the closest lepton or jet vs. $\not{E}_T$ for the $e\mu$ candidates. Upper left: all-jet multiplicities. Upper right: zero-jet events. Lower left: one-jet events. Lower right: $\geq$ 2-jet events (signal region).

detector effects smear the resolution. The mean of this distribution is $\sim 2000\ \mu m$, while the expected resolution on this quantity is about $\sim 150\ \mu m$.

The SVX-tagging algorithm begins by selecting displaced tracks in a cone of radius $\sqrt{\Delta\eta^2 + \Delta\phi^2} = 0.4$ about the axis of a given jet. The tracks are required to have impact parameter significance $\frac{d}{\sigma_d} \geq 2.5$, and $P_T \geq 0.5\ GeV/c$. The algorithm then attempts to find a displaced vertex with three or more tracks. If this fails, the track requirements are tightened to $\frac{d}{\sigma_d} \geq 4.0$, and $P_T \geq 1.5\ GeV/c$, and the algorithm attempts to find a displaced vertex with only two tracks. In each case, the criteria for a tag is that the transverse decay length be greater than three times its uncertainty: $L_{xy}/\sigma_{L_{xy}} > 3.0$. From Monte Carlo studies, we find that the algorithm tags $(42 \pm 5)\%$ of all top events passing the lepton plus jets selection criteria. The expected number of events from $t\bar{t}$ passing all cuts is shown in Table 3, for a luminosity of $100\ pb^{-1}$.

The background to b-tagged events comes primarily from inclusive QCD W events containing real heavy flavor. The processes which contribute are $p\bar{p} \to Wg$ ($g \to b\bar{b}$, $c\bar{c}$) and $p\bar{p} \to Wc$. In addition, there are contributions to the background from fake tags (i.e., tags in events which contain no true displaced

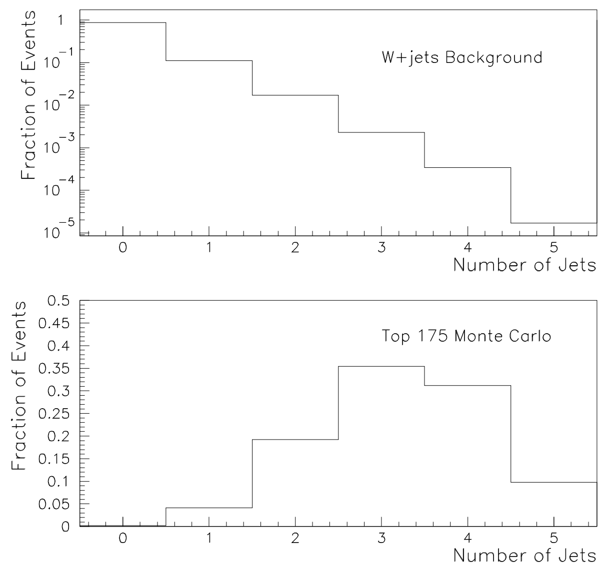

Fig. 7. Fraction of events vs. jet multiplicity observed in W plus jets data. The bottom plot shows the distribution expected from $t\bar{t}$ Monte Carlo with $M_{top} = 175\ GeV/c^2$.

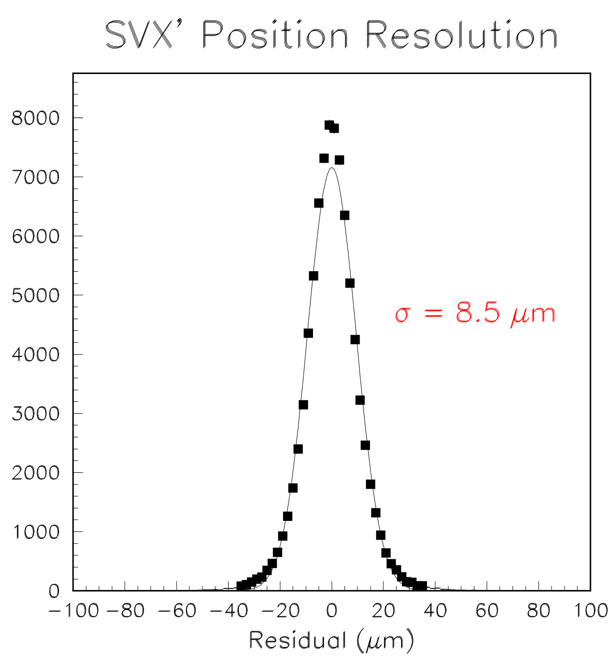

Fig. 8. Tracking residuals for all four layers of the SVX.

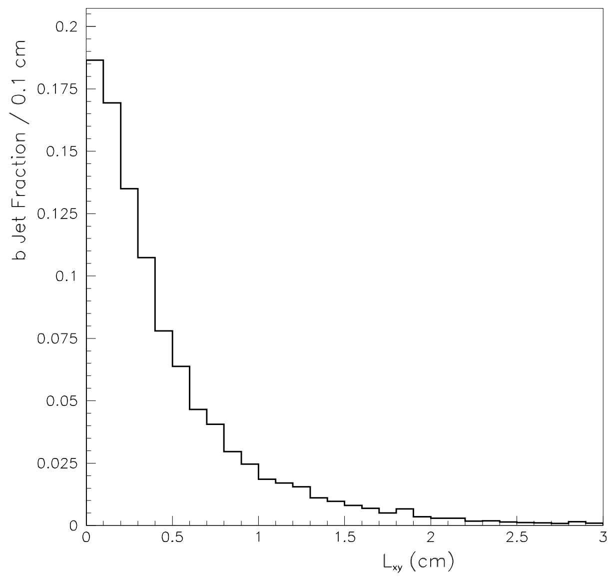

Fig. 9. The transverse decay length distribution for b hadrons, before detector resolution effects, from $t\bar{t}$ Monte Carlo events with $M_{top} = 175\ GeV/c^2$.

Top Mass (GeV/c^2)	$\sigma_{t\bar{t}}$ (pb)	Expected Events (above background)
160	8.2	30
170	5.8	24
180	4.2	15

Table 3. The predicted central value of the $t\bar{t}$ production cross section from Laenen *et al.*, and the number of SVX-tagged lepton plus jets $t\bar{t}$ events expected in 100 pb^{-1} after all cuts, as a function of top-quark mass.

vertices), and a small component from the following processes: $Z \to \tau\tau$, non-W, WW, WZ, and Drell-Yan.

Monte Carlo is used to determine the fraction of observed W + jet events containing $Wb\bar{b}, Wc\bar{c}$, and Wc. The tagging efficiency as measured in the data is then used to calculate the expected number of tags from these sources. The background from mis-tags is determined from a parameterization of fake tags observed in "generic" QCD jet data. The additional backgrounds are derived from a combination of data and Monte Carlo.

	Before Tag	Total Background	Observed Tags (Events)
W+0 Jet	88049		
W+1 Jet	9531	74.5±16.9	61 (61)
W+2 Jet	1469	29.7±7.9	43 (38)
W+ $\geq$ 3 Jet	296	9.9±2.8	40 (32)

Table 4. Observed SVX-tags in the W + jets sample, compared with expected background, vs. jet multiplicity bin. The signal region for $t\bar{t}$ is the W + $\geq$ 3 jet sample.

The total background is calculated separately for each W jet multiplicity bin. The results are shown in Table 4, along with the number of tags observed in the data. In the $W + 1$ jet bin, where we expect little contribution from top, there is good agreement between the observed tags and the calculated background. There is a small excess of tags in the $W + 2$ bin, consistent with the background estimate plus a small contribution from top. In the signal region of $W+ \geq 3$ jets, we observed 40 tags in 32 events over a total background of 9.9 ± 2.8 tags. A plot of observed tags and background, vs. W jet multiplicity, is shown in Fig. 10.

We have examined a number of features of the tagged events. The hypothesis is that the tagged events represent $t\bar{t}$ events where one W from a top decays to a lepton and a neutrino. In Fig. 11, we compare the transverse mass (computed using the x and y components of the lepton and $\not\!\!E_T$ in the event) observed for the tagged events vs. the distribution expected from a Monte Carlo for $M_{top} = 175\ GeV/c^2$. The agreement is good. We have the $\mathcal{H}$. In Fig. 12, we see good agreement between the $\mathcal{H}$ (described below) observed in the tagged events and the distribution expected from $t\bar{t}$ Monte Carlo plus background. In Fig. 13, we also see good agreement between E_T of the tagged jets observed in the data and the distribution expected from $t\bar{t}$ Monte Carlo plus background. Finally, we can also examine observed tags vs. expected background in the Z + jets sample. There is very little contribution from top expected in this sample,[16] although there is a large reduction in statistics relative to the W + jets sample. The results are shown in Table 5. There is good agreement between tags and background in each jet multiplicity bin.

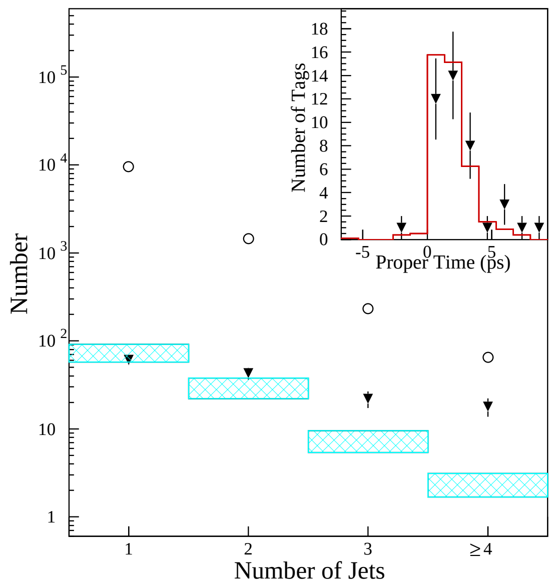

Fig. 10. The W + jets distribution observed in the data. The open circles are before SVX-tagging and the solid triangles are after SVX-tagging. The hatched boxes represent the tagging background estimate. The inset compares the $c\tau$ of the tagged jets in the W + $\geq$ 3 jet sample with the distribution observed in top Monte Carlo.

3.2 Soft Lepton Tagging

The second method used to tag b quarks in top events is to identify electrons and muons from b decay. The leptons are referred to as *soft* due to the low momentum requirement of $P_T \geq 2\ GeV$. These additional leptons come primarily from the process $b \rightarrow \ell\nu X$ and the cascade process $b \rightarrow cX$, $c \rightarrow \ell\nu X$, but also from decays such as $W \rightarrow c\bar{s}$, $c \rightarrow \ell\nu X$ and $W \rightarrow \tau\nu$, $\tau \rightarrow \ell\nu\nu$.

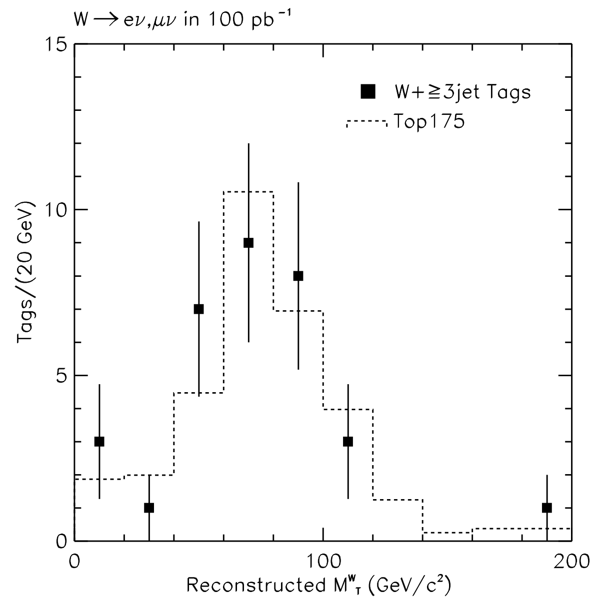

Fig. 11. Transverse mass of the SVX-tagged $W+\geq 3$ jet events (points) compared with shape expected from top Monte Carlo (solid histogram).

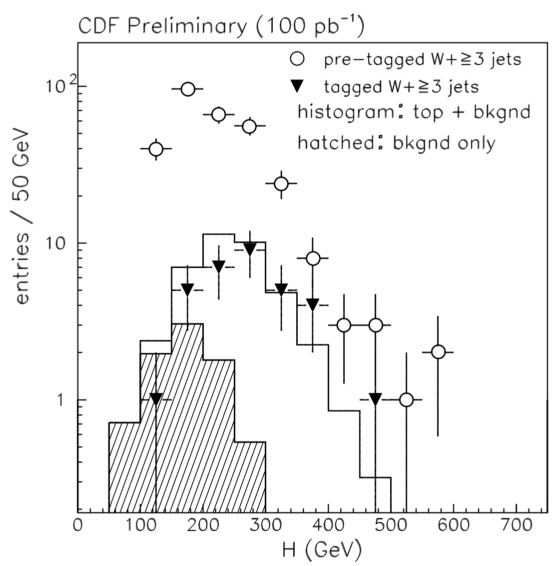

Fig. 12. $\mathcal{H}$ distributions for pretagged $W+\ \geq 3$ jet events (open circles), SVX-tagged $W+\ \geq\ 3$ jet events (solid triangles), compared to tags in top plus background Monte Carlo (solid histogram), and tags in background-only Monte Carlo (hatched histogram).

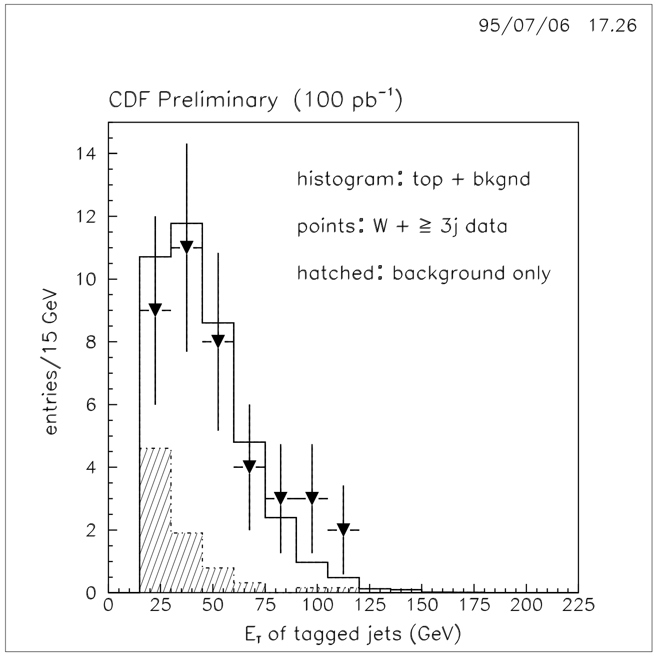

Fig. 13. SVX-tagged jet E_t of the tagged $W + \geq 3$ jet events (solid triangles), compared to tags in top plus background Monte Carlo (solid histogram), and tags in background only Monte Carlo (hatched histogram).

	Total Background	Observed Tags
$Z+1$	8.4 ± 0.84	6
$Z+2$	2.3 ± 0.23	3
$Z+\geq 3$	0.94 ± 0.09	1

Table 5. Observed SVX-tags in the $Z +$ jets sample, compared with expected background, vs. jet multiplicity bin.

The efficiency for identifying electrons is measured in the data using photon conversions $\gamma \rightarrow e^+e^-$. The efficiency for identifying muons is measured in the data using J/ψ, $Z \rightarrow \mu^+\mu^-$ events. The efficiency for finding an additional e or μ in a $t\bar{t}$ event passing the lepton plus jets selection criteria is (20±2)%. The primary background (about 75%) for soft lepton tags are hadrons misidentified as leptons, and electrons from unidentified photon conversions. A smaller background comes from processes which generate real heavy flavor, such as $Wb\bar{b}$ and $Wc\bar{c}$. The rate for these backgrounds is measured using generic jet samples and parameterized as a function of the P_T of the lepton candidates. Other much smaller backgrounds are calculated in the same manner as for the SVX analysis.

As before, the total background is calculated separately for each W jet multiplicity bin. The results are shown in Table 6, along with the number of SLT-tags observed in the data. There is good agreement between the observed tags and the calculated background in the $W+1$ and $W+2$ jet bins. In the signal region of $W+\geq 3$ jets, we observe 40 SLT-tags in 36 events over a total background of 23.8 ± 3.6 tags. A plot of observed tags and background vs. W jet multiplicity is shown in Fig. 14.

	Before Tag	Total Background	Observed Tags
W+0 Jet	88049		
W+1 Jet	9531	250±38	232
W+2 Jet	1469	71±11	84
W+$\geq$ 3 Jet	296	23.8±3.6	40

Table 6. Observed SLT-tags in the $W+$ jets sample, compared with expected background, vs. jet multiplicity bin. The signal region for $t\bar{t}$ is the $W+\geq 3$ jet sample.

4 Measurement of the $t\bar{t}$ Production Cross Section

We calculate the cross section implied by the excess of events observed in the three counting experiments: $W+$jets with an SVX B-tag, $W+$jets with an SLT

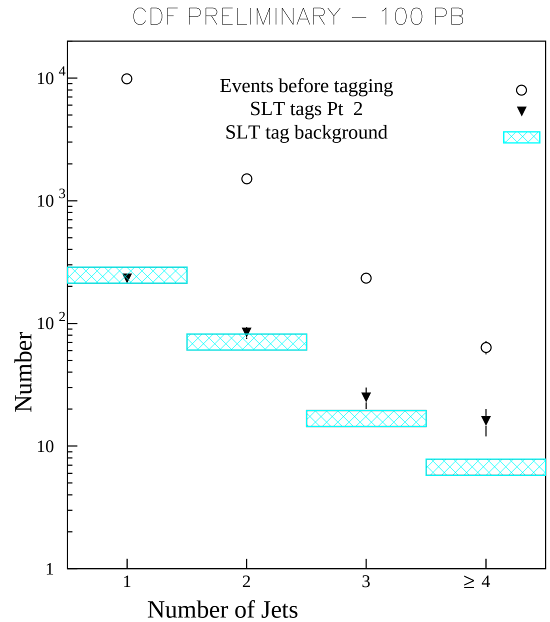

Fig. 14. The W + jets distribution observed in the data. The open circles are before SLT tagging and the solid triangles are after SLT tagging. The hatched boxes represent the tagging background estimate.

B-tag, and dileptons. The cross section is calculated using the relation:

$$\sigma = \frac{n - b}{\epsilon^{tot} \cdot \int \mathcal{L} dt}$$

where n is the observed number of events, b is the estimated background, and ϵ^{tot} is the total acceptance (including branching ratios) for a given channel. $\int \mathcal{L} dt$ is the integrated luminosity, and for the result stated below it is 67 pb^{-1}. The cross section is determined by maximizing the likelihood expression:

$$L = G(\int \mathcal{L}dt, \overline{\int \mathcal{L}dt}, \sigma_{\int \mathcal{L}dt}) \cdot L^{SVX} \cdot L^{SLT} \cdot L^{DIL}$$

and

$$L^i = G(\epsilon, \bar{\epsilon}, \sigma_\epsilon) \cdot G(b, \bar{b}, \sigma_b) \cdot P(n, \epsilon \cdot \int \mathcal{L}dt \cdot \sigma + b),$$

where $i = SVX$, SLT, and DIL, $G\ (p, \bar{p}, \sigma_p)$ is a Gaussian for parameter p, with mean $\bar{p}$ and width σ_p, and $P\ (n, m)$ is a Poisson with mean m and number of observed events n. The quantities ϵ and b represent the total efficiency and background for a given channel i. In practice, the above expressions are separated into pieces that either are or are not common between Run 1A and Run 1B.

Item	SVX	SLT	Dilepton
N_{events}^{tagged}	21	22	7
ϵ_{total} (in %)	3.4 ± 0.9	1.7 ± 0.3	0.78 ± 0.08
Background	5.5 ± 1.8	14.7 ± 2.2	1.3 ± 0.3
Luminosity	$67 \pm 5\ pb^{-1}$	$67 \pm 5\ pb^{-1}$	$67 \pm 5\ pb^{-1}$

Table 7. Parameters used in the calculation of the combined SVX/SLT/dilepton $t\bar{t}$ production cross section.

In addition, the acceptance for the SVX and SLT channels, before tagging, is taken as 100% correlated. A subset of the parameters used in the calculation are listed in Table 7. Note that the background in the SVX and SLT channels have been corrected for the top content in the sample before tagging using an iterative technique.[17] Combining the three channels results in $\sigma(t\bar{t}) = 7.6\ ^{+2.4}_{-2.0}\ pb$. In Fig. 15, we compare this result, along with the CDF measurement of the top-quark mass (described below), vs. the theoretical expectation.

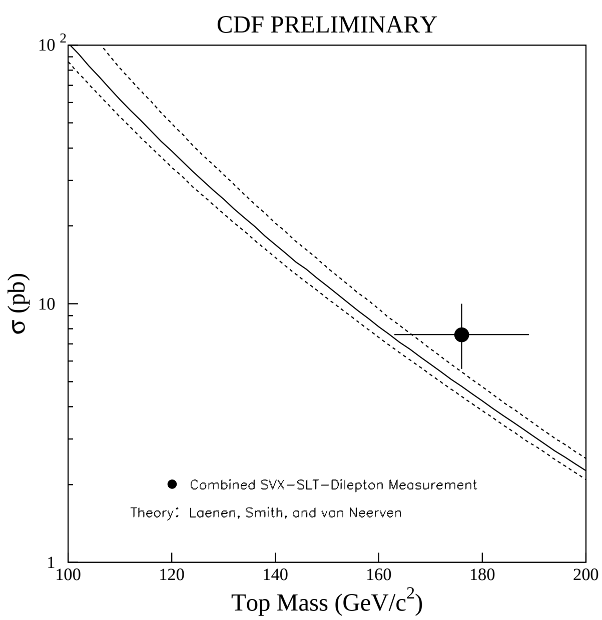

Fig. 15. Comparison of the CDF measurements of the $t\bar{t}$ production cross section and the top-quark mass, vs. the expectation of theory, from Laenen *et al.*

5 Determination of V_{tb}

In the Standard Model, a 176 GeV/c^2 top quark decays almost exclusively to Wb, because $V_{tb} \sim 1$ and there is no kinematic suppression of this decay. In fact, the statement that $V_{tb} \sim 1$ assumes that the CKM matrix is 3×3 and unitary, and this is something we would like to test. The procedure used to measure V_{tb} is relatively straightforward. We measure the ratio:

$$b = \frac{BF(t \to Wb)}{BF(t \to Wq)} = \frac{V_{tb}^2}{V_{td}^2 + V_{ts}^2 + V_{tb}^2},$$

where the relative branching fraction of top to Wb is measured by examining the distribution of dilepton events with zero, one, and two b-tagged jets, and by examining the distribution of lepton plus ≥ 3 jets events with one and two b-tagged jets. This technique takes advantage of the fact that values of $BF\ (t \to Wb)$ significantly smaller than 1.0 would have a noticeable effect on the relative distribution of events in each category. A maximum likelihood estimator is used to determine the best fit ratio, and in 100 pb^{-1}, we find

$$b = \frac{BF(t \to Wb)}{BF(t \to Wq)} = 0.94\ \pm 0.27(stat)\ \pm 0.13(syst)$$

and at 95% CL, we obtain $b > 0.34$.

We then use the above relation to determine V_{tb}. Assuming unitarity, we obtain $|V_{tb}| = 0.97 \pm 0.15 \pm 0.07$. Additionally, we can relax the assumption of three-generation unitarity. Assuming that there is no coupling between the first two and a possible fourth generation, then $|V_{td}| = 0.004 - 0.015$ and $|V_{ts}| = 0.030 - 0.048$ (Ref. 18). To extract a 95% CL limit on $|V_{tb}|$, we assume that $|V_{td}|$ and $|V_{ts}|$ take on their smallest allowed values, and use our 95% CL limit measurement of b. We find that at 95% CL, $|V_{tb}|\ >\ 0.022$ (95% CL).

6 Top-Mass Reconstruction

We measure the top-quark mass using the $W+ \geq 3$ jet events which also contain at least one additional jet with $E_T > 8$ GeV, $|\eta| < 2.4$. This sample will be referred to as the $W+ \geq 4$ jet sample. This sample can then be fit to the hypothesis:

$$
\begin{aligned}
&p\bar{p} \rightarrow t_1 + t_2 + X \\
&t_1 \rightarrow W_1 + b_1 \\
&t_2 \rightarrow W_2 + b_2 \\
&W_1 \rightarrow l + \nu \\
&W_2 \rightarrow j_1 + j_2,
\end{aligned}
$$

assuming the four highest E_T jets correspond to the partons b_1, b_2, j_1, and j_2. When calculating masses, all jet energies are corrected for detector effects, for contributions from the underlying event, and for energy falling outside of the fixed cone size of 0.4. Finally, there are specific corrections for jets tagged as b's. When tagging information is required, both SLT and SVX-tagged events are used. All possible assignments of jets to partons are tried, with the restriction that if a jet is tagged, it is required to be one of the b jets. The $\not{E}_T$ is assumed to represent the transverse components of the neutrino, and the constraint that the lepton and $\not{E}_T$ reconstruct to the W mass yields a two-fold ambiguity for the P_z of the neutrino. The two jets selected as the decay products of the hadronic W are also constrained to the W mass. Finally, both top masses (representing the hadronic and leptonic W decays) are required to be the same. Within estimated uncertainties, the jet energies are allowed to vary in order to satisfy the constraints. Each particular assignment of jets to partons yields a top mass and a χ^2, and the solution with the lowest χ^2 is chosen for each event. This χ^2 is required to be less than ten. The resulting distribution of top masses observed in the data is then compared to the expectation for top plus background for various top masses. The background shape is from Monte Carlo W + jet events satisfying the same selection criteria as the data, and the normalization is fixed using a method described in our previous publication.[7]

In 67 pb^{-1}, there are 99 $W + \geq 4$ jet events using the criteria described above. There are 19 events which contained either an SVX or SLT tag, of which $6.3^{+2.1}_{-1.7}$ are expected to be background. Figure 16 shows the data along with the best fit expectation for signal plus background. The inset shows the negative ln (likelihood) returned by the fit at each top mass. The minimum of the negative ln (likelihood) yields the best fit, and a change in the ln (likelihood) of 0.5 gives the statistical uncertainty. The systematic uncertainties are extrapolated from our earlier publication,[7] the dominant sources being the effects of gluon radiation on the determination of parton energies, and the jet energy scale. The final result for the mass is $M_{top} = 176 \pm 8(stat) \pm 10(syst)\ GeV/c^2$. In Fig. 17, we show the reconstructed mass distribution for the sample of $W + \geq 4$ jet events before b-tagging. This distribution also shows an excess of events over the background shape in the region of reconstructed mass $\sim 175\ GeV/c^2$.

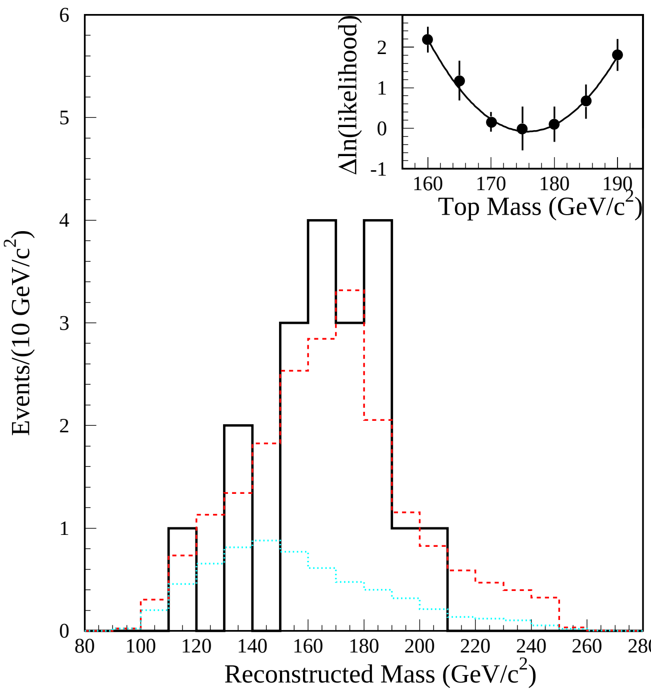

Fig. 16. Reconstructed mass distribution for events containing at least one SVX or SLT b-tagged jet. The dashed histograms represent the fitted distributions from background and the sum of background and signal. The inset plot shows the likelihood for similar fits to different top-mass hypotheses.

We have also looked for evidence of the decay of the hadronic W in this sample. In the first method, we use the same mass fitting procedure described above, except that we release the constraint on the hadronic W decay. We can then examine the mass distribution of the jets the fitter chooses (for the minimum χ^2 solution) as the decay products of the hadronic W. In Fig. 18, we can see a clear excess of events in the region of the W mass.

The second method takes advantage of the fact that when both b quarks are tagged, there is a unique jet-jet mass combination for the W decay. Both SVX and SLT tags are used, although the criteria for an SVX tag are loosened to improve acceptance. In 100 pb^{-1}, ten events satisfy these selection criteria. The mass distribution for the remaining two non-b jets is shown in Fig. 19. A clear peak is seen at the W mass.

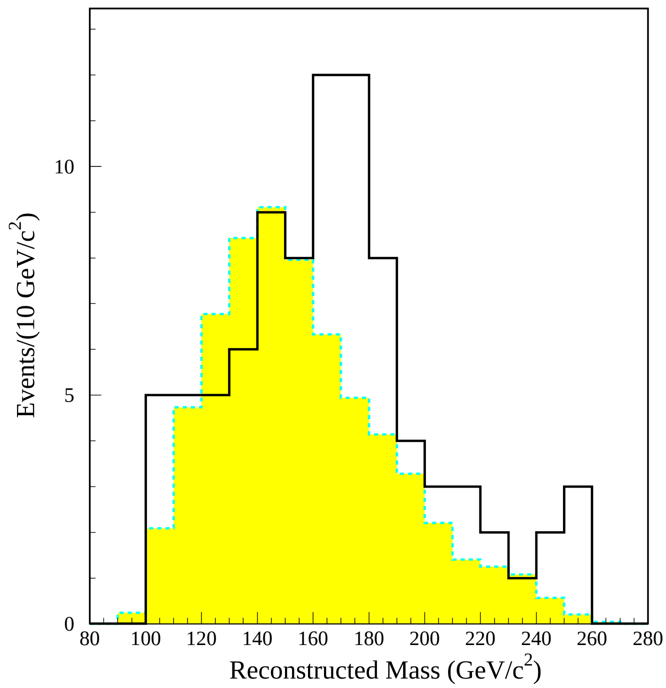

Fig. 17. Reconstructed mass distribution for the sample of W + 4 jet events before b-tagging. The shaded histogram is that expected for background with the normalization taken from a fit made with a background constraint.

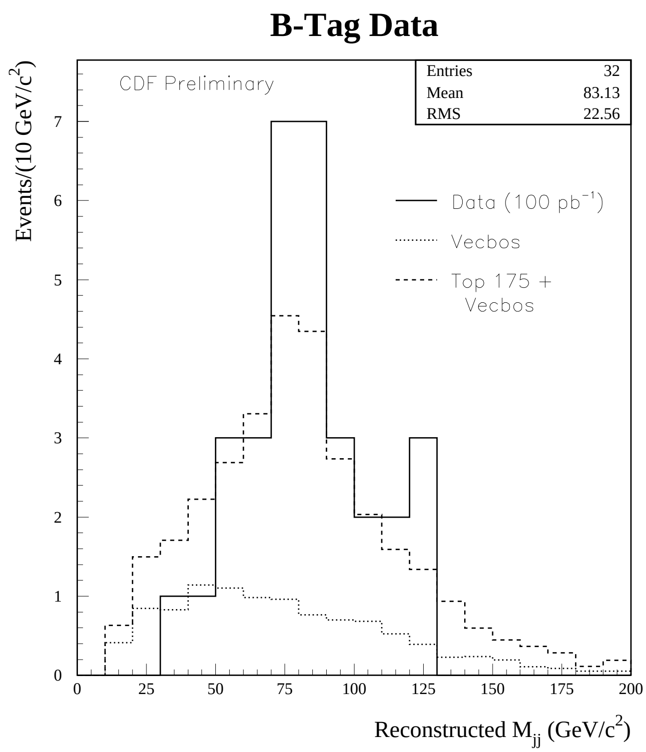

Fig. 18. Plot of the invariant mass of the two jets assigned as the decay jets of the hadronic W, when the W mass constraint is removed from the fit. Note the excess of events in the region of the W mass.

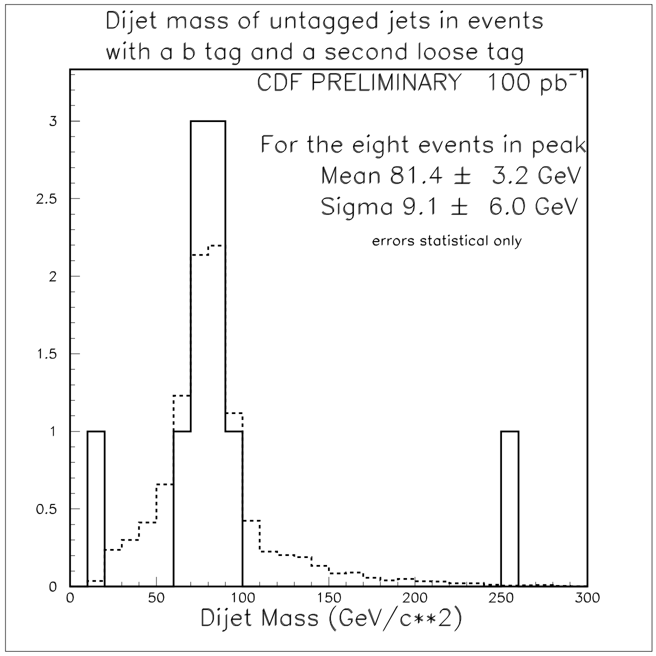

Fig. 19. Dijet mass distribution of untagged jets in events with two identified b quarks. The solid curve is for the ten events observed in the data, and the dashed curve is for a Monte Carlo calculation.

7 The $t\bar{t}$ Invariant Mass

As a result of the constrained fit in the lepton plus jets sample, one obtains the four-momenta of the t and the $\bar{t}$ quarks. Using these quantities, we can then calculate the $t\bar{t}$ invariant mass for each event. This quantity is sensitive to non-Standard Model top quark production mechanisms. A number of authors[19,20] have pointed out the possibility of heavy resonances which could have sizable decay branching ratios to $t\bar{t}$. In determining this quantity, an improvement in resolution of a factor of ≈ 2 can be obtained by constraining the top mass to the value measured in the previous section. The resulting distribution observed in 100 pb^{-1} is shown in Fig. 20. The data shows good agreement with the shape expected from Standard Model $t\bar{t}$ plus background. In order to gain acceptance, we can perform the same analysis using the pretagged data. This is shown in Fig. 21, and once again, there is good agreement between data and Standard Model $t\bar{t}$ plus background.

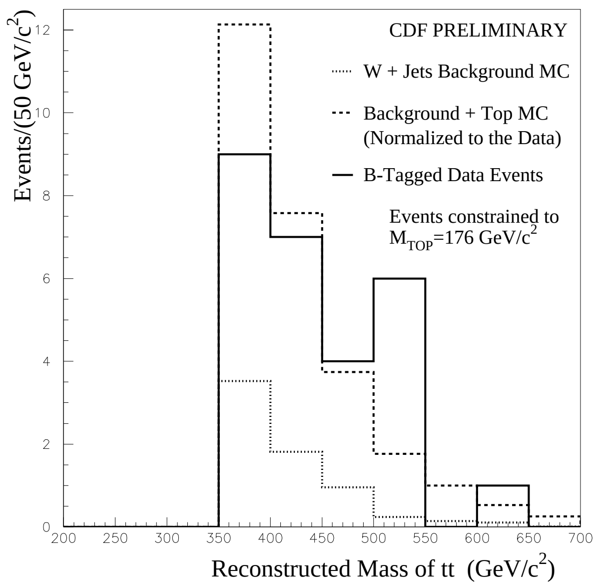

Fig. 20. $t\bar{t}$ invariant mass after b-tagging for the data (solid histogram), W + jets Monte Carlo normalized to the expected background rate (dotted histogram), and top plus W + jets Monte Carlo (dashed histogram).

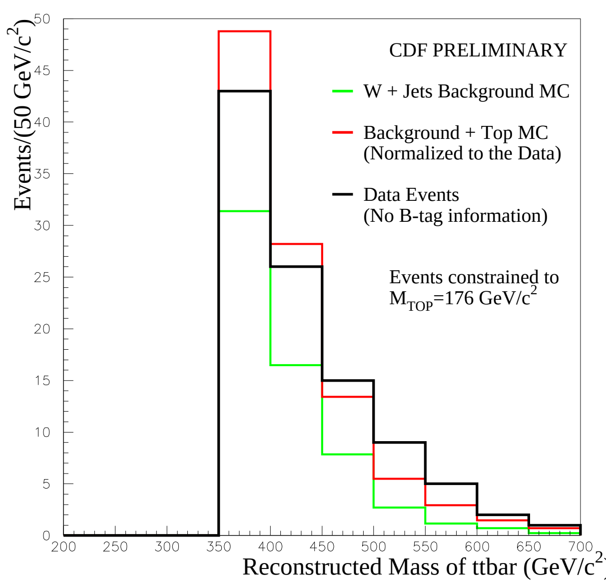

Fig. 21. $t\bar{t}$ invariant mass before b-tagging for the data (solid histogram), W + jets Monte Carlo normalized to the expected background rate (dotted histogram), and top plus W + jets Monte Carlo (dashed histogram).

8 The $\mathcal{H}$ Analysis

Due to the large top-quark mass, $t\bar{t}$ events are produced with large $\sqrt{s}$ compared to background processes. A simple variable which scales with $\sqrt{s}$ is $\mathcal{H}$, which is defined as

$$\mathcal{H} = E_T(lepton) + \not{E}_T + \sum_{jets} E_T(jets),$$

where the sum over jets includes all jets with $E_T \geq 8\ GeV$ and $|\eta| \leq 2.4$. This analysis is performed on the pretagged mass sample. A feature of this analysis is that it is sensitive to non-b tagged top events, as well as providing an independent check of M_{top} and $\sigma(t\bar{t})$.

In Fig. 22, we show the separation obtained using $\mathcal{H}$, for $t\bar{t}$ Monte Carlo vs. W + 4 jet background. Also shown in this figure is the distribution of $\mathcal{H}$ observed in the full data sample, as well as for the subset of events containing a b tag. These events cluster near large $\mathcal{H}$ as expected for the $t\bar{t}$ component of the distribution. We perform a two-component binned maximum-likelihood fit of the $\mathcal{H}$ distribution of this sample, to a sum of distributions expected for $t\bar{t}$ and background. As in the mass reconstruction analysis, this is done for several values of top mass. The resulting negative ln(likelihood) vs. top mass is plotted in Fig. 23. The top mass we obtain using 99 events in 67 pb^{-1} is $M_{top} = 180 \pm 12(stat)^{+19}_{-15}(syst)\ GeV/c^2$, which is in good agreement with the mass determination from the lepton plus jets sample.

9 The All-Hadronic Channel

The selection for this channel is based on the expected decay topology $t\bar{t} \rightarrow W^+bW^-\bar{b} \rightarrow q\bar{q}'\ q\bar{q}'\ \ b\bar{b}$. Each event is required to pass the following criteria:

- $N_{jet} \geq 6$, where N_{jet} is the number of jets with $E_T > 15\ GeV$ and $|\eta| < 2.0$. The jets must be separated in η, ϕ space by $\Delta R_{min} \geq 0.5$.
- $\sum E_T \geq 150\ GeV$, where $\sum E_T$ is the transverse energy sum over the N_{jet} jets.
- $\sum E_T/\sqrt{s} \geq 0.75$.
- $A \geq -0.003 \times \sum E_T + 0.45$, where A is aplanarity calculated in the center-of-mass system of the N_{jet} jets.
- Require at least one SVX-tagged jet.

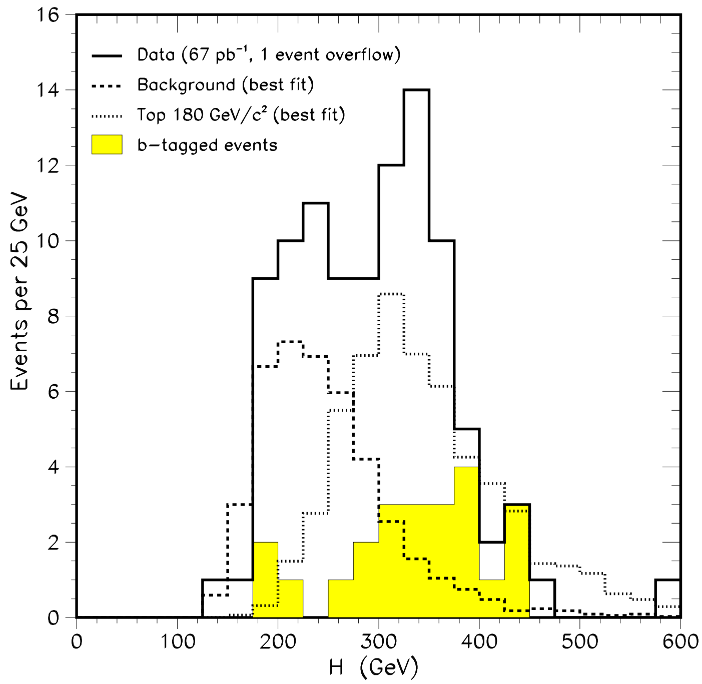

Fig. 22. $\mathcal{H}$ distribution of CDF data (solid line), W + 4 jet background (dashed line), and $t\bar{t}$ Monte Carlo with $M_{top} = 180\ GeV/c^2$ (dotted line). The shaded distribution shows the events in the data containing a b tag.

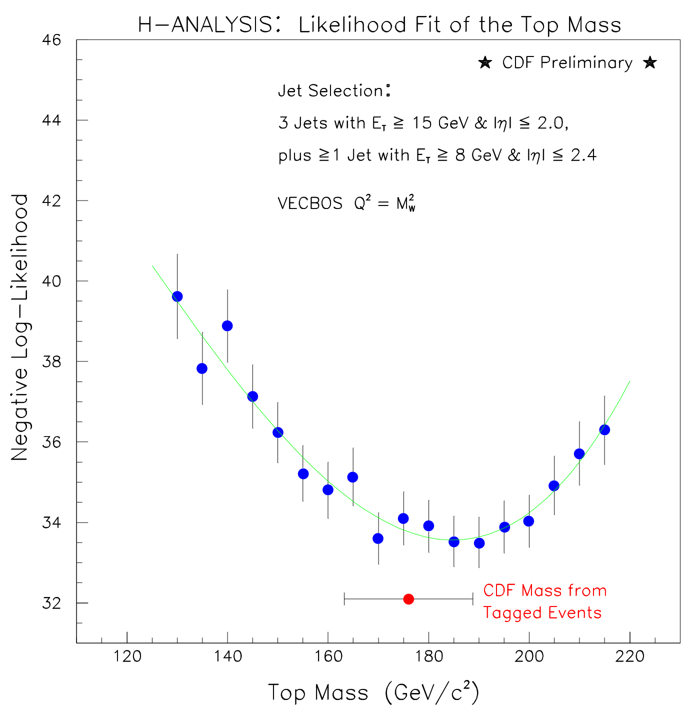

Fig. 23. Resulting negative ln(likelihood) vs. top mass for fits of $\mathcal{H}$ distribution of CDF data to a sum of distributions expected for $t\bar{t}$ and background. Also shown is the CDF mass result from the $W+ \geq 4$ jet sample described earlier.

The efficiency for this selection (including all decay modes) is $\epsilon_{HAD} = (8.6 \pm 0.4(stat))\%$ for $M_{top} = 175\ GeV/c^2$. The data comes from a multijet trigger, and the results below are based on an integrated luminosity of $\mathcal{L} = 81\ pb^{-1}$.

These events are then fit to the $t\bar{t}$ hypothesis using a method similar to that described above. Each of the six highest E_T jets is assigned as one of the six decay partons of the t and $\bar{t}$. Momentum conservation is required at the two top decay vertices, and the masses of the resulting t and $\bar{t}$ from the fit are constrained to be equal. The two W mass constraints are not imposed so as to reduce the total number of combinations. The solution with the best χ^2 is chosen.

We have used two methods to determine the shape of the background mass spectrum. The first method uses events which pass all of the selection criteria, but which contain no SVX-tagged jet. This sample is expected to contain less than 5% $t\bar{t}$ signal. The background distribution is shown in Fig. 24. In the second method, we parameterize the tag rate (as observed in an independent sample) and apply it event by event to the pretagged multijet sample. This procedure should include any biases on the background mass spectrum due to the tagging itself. The resulting shapes of the background from the two methods are in excellent agreement and are shown in Fig. 24. We have found that a Landau-like distribution adequately models the shape of the background and use this in our fit. The mass distribution observed in the data is then fit to a sum of the Landau describing the background, and a Gaussian distribution describing the $t\bar{t}$ signal. The normalization of the background and top components are left free in the fit. The result of the fit is shown in Fig. 25. The mean of the Gaussian yields a top mass in good agreement with the result of lepton plus jets analysis. From the fit result for the number of top events, the acceptance quoted above, and the integrated luminosity of the multijet sample, we calculate the $t\bar{t}$ production cross section to be:

$$\sigma_{t\bar{t}} = 9.6 \pm 3.5 \text{ (stat. only) } pb,$$

also in good agreement with the cross-section result from the SVX, SLT, and dilepton channels quoted earlier.

10 The Future for Top at CDF

The current limiting factor to higher luminosities at the Tevatron is the total number of antiprotons in the ring. Fermilab is currently building a new Main

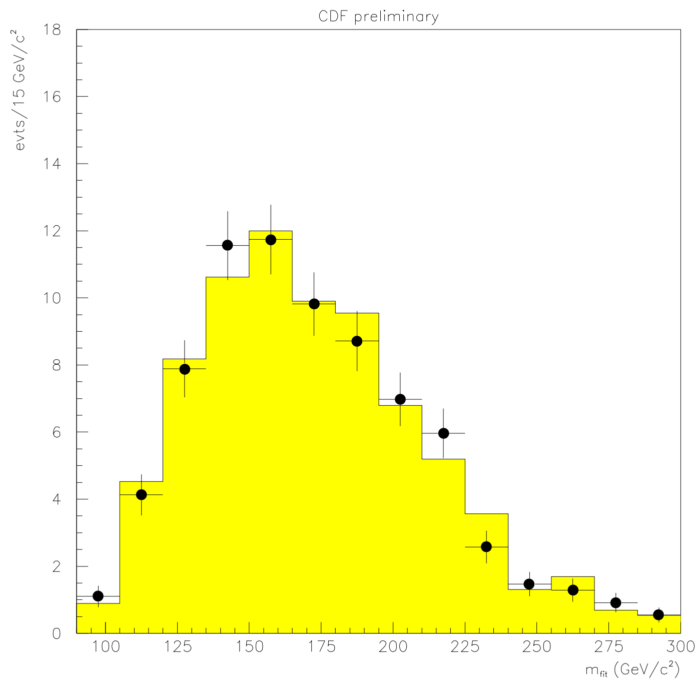

Fig. 24. Background mass distribution for the all-hadronic analysis. The points are from the no b-tag sample, and the shaded histogram is from the tag rate parameterization.

Injector accelerator that will lead to antiproton production rates about a factor of two above what is currently possible. It will also improve the transfer efficiency for antiprotons. This should lead to instantaneous luminosities of roughly a factor of four over what can currently be attained. In addition, a proposed device called the Recycler Ring may allow more efficient production and use of antiprotons, and could yield another factor of two to three in instantaneous luminosity. Finally, the beam energy will be increased from the current 900 GeV to 1000 GeV in Run II. Some parameters of the current and future Tevatron are listed in Table 8.

Run	Energy (GeV)	Instant Lum. ($cm^{-2}sec^{-1}$)	Integ. Lum. (pb^{-1}/week)
1B (Present)	900	2×10^{31}	4
II (MI)	1000	8×10^{31}	17
II (MI+Recycler)	1000	20×10^{31}	41

Table 8. Performance parameters of the Tevatron in the 1994–95 run compared with expected parameters for Run II.

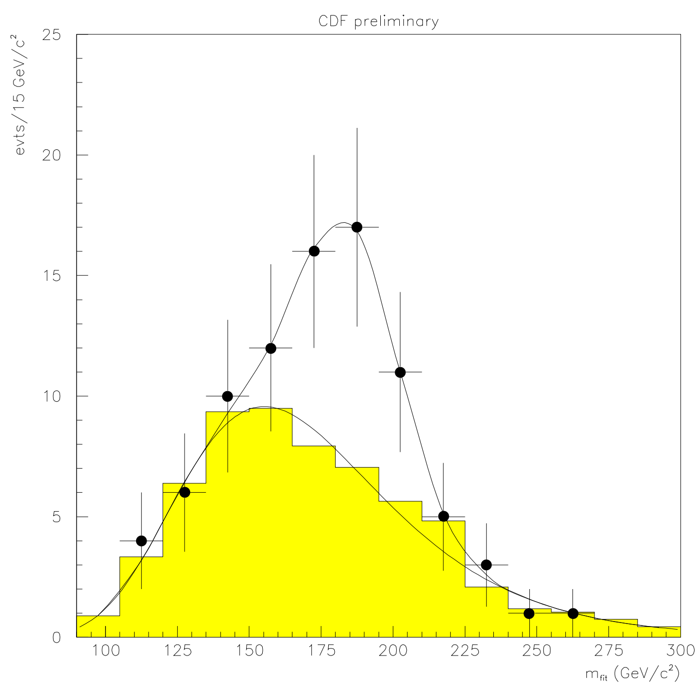

Fig. 25. Fitted top-mass distribution in the all-hadronic channel. The points are the b-tagged signal sample. The shaded histogram is the background normalized to the outcome of the fit. The lower curve is a Landau distribution representing the background shape, and the upper curve is a sum of this Landau and a Gaussian distribution representing the $t\bar{t}$ signal.

The CDF detector has been used to study proton-antiproton collisions at Fermilab since 1985. During this time, the detector has been upgraded to increase physics capability and to keep pace with changes to the Tevatron. The improvements to the Tevatron noted above necessitate replacement or modification of several detector systems. These detector systems include:

- Silicon Vertex Detector (SVX II)
  - The new detector will have five layers and will be double-sided to provide both $r - \phi$ and $r - z$ readout, allowing three-dimensional vertex reconstruction. In addition, the detector will be ~ 90 cm long, allowing much more complete coverage of the $p\bar{p}$ interaction region.
- Intermediate Fiber Tracker (IFT)
  - This will be a scintillating fiber tracker in the region $r \sim 16 - 27\ cm$. The IFT plus SVX II tracking combination should allow b-tagging out to $|\eta| = 2$, as well as improving electron identification in the region covered by the new plug calorimeter.
- Plug Calorimeter Upgrade
  - This is a scintillating-tile fiber calorimeter with a shower-max detector. It should allow for greatly improved electron identification at large rapidity.
- Muon Detection System
  - The muon detectors in the central region will have additional chambers installed to allow more complete ϕ and η coverage. In addition, the more compact design of the new plug calorimeter will allow the forward muon system to move closer to the interaction region, increasing our muon acceptance.

The above changes to the accelerator and the detector will impact the top analysis in a number of significant ways. First, at $\sqrt{s}$ =2 TeV, the $t\bar{t}$ production cross section increases by $\sim 40\%$ relative to $\sqrt{s}$ =1.8 TeV. The new plug calorimeter could increase the acceptance for $W \rightarrow e\nu$ from top by about 25%, assuming one can maintain a signal-to-noise ratio similar to what is currently achieved in the central calorimeter. Finally, one should note that the current Silicon Vertex Detector used in Run 1B only covers about 60% of the $p\bar{p}$ interaction region, while the SVX II detector will cover almost all of the $p\bar{p}$ interaction region. This will almost double the b-tagging efficiency to about 80% per top event (compared to 42% at present).

Taking all of these improvements into account, the expected yield of $t\bar{t}$ events in the lepton + 4 jets + b-tag mode (i.e., the tagged mass sample) should be $\sim$ 600 per fb^{-1} (compared to $\sim$ 200 per fb^{-1} in the current run). With yields such as these, the expected precision on a number of top measurements can be estimated. For example, with 2 fb^{-1} of data, we expect to measure the top mass to better than $\sim$ 4 GeV/c^2 (including systematic and statistical uncertainties), and the production cross section to better than $\sim$ 7%.

11 Summary

The evidence for the top quark that CDF presented in April of 1994 was confirmed in all aspects by the results of the CDF and D∅ Collaborations in March of 1995. We have observed top in a number of different decay channels. We have used the lepton plus jets decay channel to measure the top-quark mass:

$$M_{top} = 176 \pm 8 \pm 10 \ GeV/c^2.$$

In this same sample, we can observe a very clean peak of the process $W \rightarrow jj$, providing a sample of $WbWb$ events as expected for $t\bar{t}$. We have used a kinematic analysis of the lepton plus jets sample to derive a top-mass measurement in agreement with the above result. The $t\bar{t}$ production cross section is measured from the dilepton and lepton plus jets decay channels to be:

$$\sigma(t\bar{t}) = 7.6 \ ^{+2.4}_{-2.0} \ pb.$$

We have also observed top in the difficult all-hadronic decay channel, and derive mass and cross-section measurements consistent with the above two results. We are using the invariant mass distribution of the $t\bar{t}$ sample as a probe for new physics. Finally, we have performed the first direct measurement of the CKM matrix element V_{tb}.

We expect to record another $\sim$ 30 pb^{-1} of data in the fall (winter) of 1995(6). We plan to continue to improve our top analysis with new data and better understanding of systematic uncertainties. The Fermilab accelerator complex and the CDF detector are currently planning for Run II, which promises data samples at least a factor of ten larger than we now have. A important focus of Run II

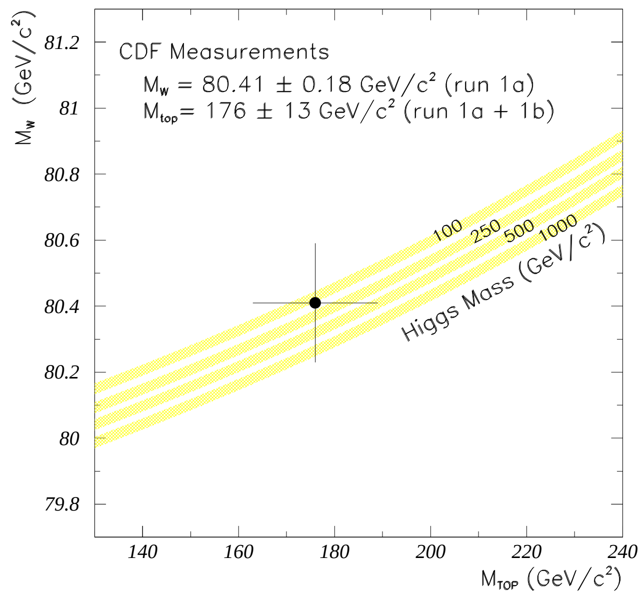

Fig. 26. Correlation between the W boson mass and the top-quark mass, for several values of the Higgs boson mass, along with current CDF measurements.

will be to probe electroweak parameter space and hopefully constrain the allowed mass range of the only unobserved Standard Model particle, the Higgs. Figure 26 shows the correlation between the W boson mass and the top-quark mass for several values of the Higgs boson mass, along with current CDF measurements.

References

[1] W. Bartel *et al.*, Phys. Lett. B **146**, 437 (1984).

[2] The LEP Collaborations ALEPH, DELPHI, L3, OPAL, and The LEP Electroweak Working Group, CERN-PPE/94-187.

[3] A. Bean *et al.*, Phys. Rev. D **35**, 3533 (1987).

[4] J. Ellis, G. L. Fogli, and E. Lisi, CERN-TH/95-202.

[5] F. Abe *et al.*, Phys. Rev. D **45**, 3921 (1991).

[6] S. Abachi *et al.*, Phys. Rev. Lett. **72**, 2138 (1994). See also S. Abachi *et al.*, Phys. Rev. Lett. **74** (1995).

[7] F. Abe *et al.*, Phys. Rev. D **50**, 2966 (1994); F. Abe *et al.*, Phys. Rev. Lett. **73**, 225 (1994).

[8] F. Abe *et al.*, Phys. Rev. D **51** (1995).

[9] F. Abe *et al.*, Phys. Rev. Lett. **74**, 2626 (1995).

[10] S. Abachi *et al.*, Phys. Rev. Lett. **74**, 2632 (1995).

[11] E. Laenen, J. Smith, and W. L. van Neerven, Phys. Lett. B **321**, 254 (1994).

[12] R. K. Ellis, in *Proceedings of the 1994 International Conference on High Energy Physics*, edited by Peter J. Bussey and Ian G. Knowles (Institute of Physics, London, 1995), p. 1203.

[13] F. Abe *et al.*, Nucl. Instrum. Methods Phys. Res., Sect. A **271**, 387 (1988).

[14] P. Azzi *et al.*, FERMILAB-CONF-94/205-E. Our previous silicon vertex detector is described in D. Amidei *et al.*, Nucl. Instrum. Methods Phys. Res., Sect. A **350**, 73 (1994).

[15] In the CDF coordinate system, θ is the polar angle with respect to the proton beam direction. The pseudorapidity, η, is defined as $-\ln\tan\frac{\theta}{2}$. The transverse momentum of a particle is $P_T = P\sin\theta$. If the magnitude of this vector is obtained using the calorimeter energy rather than the spectrometer momentum, it becomes the transverse energy (E_T). The difference between the vector sum of all the transverse energies in an event and zero is the missing transverse energy ($\not\!\!E_T$).

[16] There is a small contribution of $t\bar{t}$ to the Z sample, for $t\bar{t}$ decays to dileptons e^+e^- and $\mu^+\mu^-$, where the dilepton invariant mass falls between 75 GeV/c^2 and 105 GeV/c^2. For 100 pb^{-1}, the contribution should be less than one event.

[17] The backgrounds in these channels were both calculated under the assumption that the entire sample before tagging contains no $t\bar{t}$ component. The resulting background calculation is thus an overestimate.

[18] Review of Particle Properties, Phys. Rev. D **50**, 1315 (1994).

[19] C. T. Hill and S. J. Parke, Phys. Rev. D **49**, 4454 (1994). C. T. Hill, Phys. Lett. B **345**, 483 (1995).

[20] E. Eichten and K. Lane, Phys. Lett. B **327**, 129 (1994).